Available online at www.sciencedirect.com
ScienceDirect
European Journal of Mechanics B/Fluids 26 (2007) 650–668

Simulation of airflow fields and microparticle deposition in realistic human lung airway models. Part II: Particle transport and deposition

Zheng Li [a], Clement Kleinstreuer [b,*], Zhe Zhang [a]

[a] *Department of Mechanical and Aerospace Engineering, CFPD Lab, 3198 Broughton Hall, Campus Box 7910, North Carolina State University, Raleigh, NC 27695, USA*
[b] *Department of Mechanical and Aerospace Engineering and Department of Biomedical Engineering, CFPD Lab, 3198 Broughton Hall, Campus Box 7910, North Carolina State University, Raleigh, NC 27695, USA*

Received 26 January 2006; received in revised form 20 December 2006; accepted 13 February 2007

Available online 12 March 2007

Abstract

In Part II, given the airflow fields discussed in Part I, microparticle deposition for a practical range of Stokes numbers, $0.025 \leqslant St \leqslant 0.102$, has been simulated and analyzed, comparing different temporal assumptions, inlet conditions and geometric configurations. The matching steady-state assumption with equivalent Reynolds and Stokes numbers achieves basically the same deposition fraction (DF) values as under transient inhalation conditions. When comparing parabolic vs. realistic inlet velocity profiles, total DF-values are higher for the parabolic inlet flow for all Stokes numbers. Geometric features, such as out-of-plane configurations and cartilaginous rings in the trachea, further change local deposited microparticle concentrations when compared with simple airway models. Furthermore, significant differences were recorded when comparing DFs in some branches of the present realistic model and the Weibel Type A model. For practical purposes, algebraic microparticle-deposition correlations, $DF = DF(Re, St)$, have been obtained for both the left and right upper lung airways. Based on current research results, the out-of-plane model with tracheal rings and realistic inlet condition is recommended for future work.

Keywords: Asymmetric upper airways; Matching inlet Reynolds number; 3-D microparticle transport simulations; Particle depositions and segmental correlations

1. Introduction

Microparticle transport and deposition in the human respiratory system has been both experimentally and computationally studied, focusing on the physics of two-phase flow and applications to several research areas [1–4]. Examples include medical therapy, e.g. targeted drug aerosol delivery and the health impact of inhaled toxic particles.

Traditionally, particle trajectories and deposition fractions were simulated and analyzed for single, double or triple symmetric bifurcations [5–11], using the Weibel Type A geometry model [12]. Most recently, Ertbruggen et al. [13]

* Corresponding author. Tel.: +1 919 515 5261; fax: +1 919 515 7968.
E-mail address: ck@eos.ncsu.edu (C. Kleinstreuer).

0997-7546/$ – see front matter
doi:10.1016/j.euromechflu.2007.02.004

simulated microparticle transport using a simplified model of Horsfield et al. [14], assuming steady, uniform inlet conditions.

Experimental measurements of particle deposition have been provided by Johnston et al. [15] and Kim et al. [16,17] for single bifurcations. Based on Weibel's model, Kim et al. [18] also studied the particle deposition in a glass tube replica of a symmetric double bifurcation airway. Zhou et al. [19] measured the particle deposition in a cast of a human lung airway model with nine branches. Zhang and Finlay [20] showed experimentally that the presence of cartilaginous rings in the trachea affects local microparticle deposition.

In summary, most of these studies employed the symmetric Weibel Type A model. Geometric characteristics, such as asymmetry and spatial angle, were not fully considered. In contrast, Ertbruggen et al. [13] simulated microparticle transport in a simplified out-of-plane airway model assuming steady state, sharp carinal ridges, and uniform inlet conditions. The present computer simulation model focuses on transient effects, the geometric impact and the influence of inlet conditions. Specifically, based on the air velocity fields discussed in the accompanying Part I, one-way coupled microparticle transport and deposition are presented, using again the in-house CFPD code as described. Results for transient as well as matching steady-state micro-particle inhalation are discussed. A curve-fitted correlation has been developed to quantify particle deposition fraction as a function of inlet Reynolds number and Stokes number. Different inlet conditions, i.e., parabolic versus realistic velocity profiles plus the associated particle distributions, are discussed in conjunction with geometric influences, i.e., in-plane and out-of-plane configurations as well as tracheal rings. Exhalation is not considered because particle deposition occurs mainly during the inhalation period in the upper lung airways [21]. In addition, any influence from exhalation on the inhalation flow field mainly exists during the initial stage of the inhalation period [22]. Thus, mechanisms like "steady streaming" [23] or "trap and release" [24] are not considered in this work.

2. Theory

2.1. Airway geometry and inhalation waveform

The geometries of representative human lung airways have been introduced in Part I. The information can be summarized as follows. The model relies on data from a resin cast provided by Horsfield et al. [14]. They measured the geometric properties from the trachea to the respiratory bronchioles. The values of spatial angles were adopted from Raabe et al. [25], Thus, the present models, featuring both out-of-plane and in-plane configurations as well as tracheal rings [20], is sufficient to mimic representative human lung airways (see Figs. 1(a)–1(c)).

For the transient analysis, a realistic inhalation waveform under resting condition, as provided by Zhang and Kleinstreuer [22], was implemented (Fig. 1(d)). The maximum Reynolds number ($Re_{\text{in}} = \bar{U} D_{\text{trachea}}/\upsilon$) was about 1545 while its mean value was 1201, i.e., $Q_{\text{in}} = 15$ l/min, and $Re_{\text{match}} = 1468$ (see Section 2.3). Briefly, for the matching inlet Reynolds number, steady-state airflow patterns and especially segmentally averaged microparticle depositions match closely results obtained from transient fluid-particle flow simulations. The Stokes number range covering both toxic and therapeutic microparticles was $0.025 \leqslant St \leqslant 0.102$. A typical inhalation waveform and airway models with lettered bifurcation regions are given in Figs. 1(d) and 1(a), respectively.

2.2. Microparticle transport and deposition equations

Considering the drag to be the dominant particle point-force [22,26,34], the trajectory equation reads:

$$m_p \frac{\mathrm{d}^2 \vec{x}_p}{\mathrm{d}t^2} = \frac{1}{8}\pi d_p^2 \rho C_{DP}(\vec{v} - \vec{v}_p)|\vec{v} - \vec{v}_p| \tag{1}$$

where m_p is the mass of one particle, $\vec{x}_p$ is the displacement, d_p is the particle diameter, $\vec{v}$ is the air velocity, $\vec{v}_p$ is the particle velocity, and C_{DP} is the drag coefficient. It is defined as [26]:

$$C_{DP} = \frac{C_D}{C_{\text{slip}}} \tag{2}$$

where

$$C_D = \begin{cases} 24/Re_p & \text{for } 0.0 < Re_p < 1.0, \\ 24/Re_p^{0.646} & \text{for } 1.0 < Re_p < 400 \end{cases} \tag{3}$$

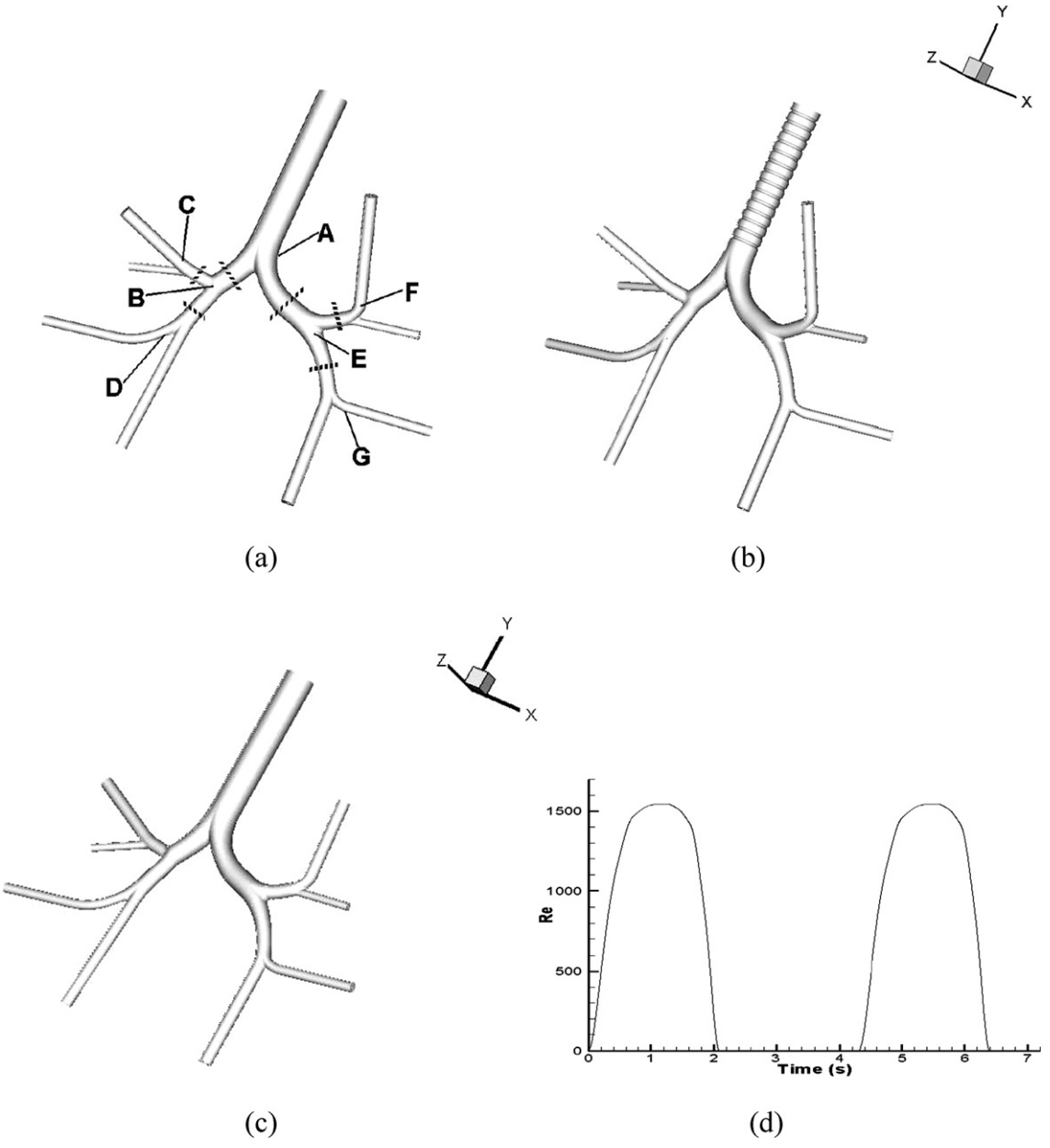

Fig. 1. Inlet waveform and airway model: (a) out-of-plane airway model (without tracheal rings); (b) out-of-plane airway model (with trachea rings); (c) in-plane airway model; (d) inhalation waveform.

and

$$Re_p = d_p \rho |\vec{v} - \vec{v}_p| / \mu, \tag{4}$$

with μ being the dynamic viscosity of the fluid. The correlation for the slip factor, C_{slip}, is also given by Clift et al. [26]:

$$C_{\text{slip}} = 1 + \frac{2\lambda_m}{d_p}\left[1.142 + 0.058\exp\left(-0.999\frac{\mathrm{d}_p}{2\lambda_m}\right)\right] \tag{5}$$

where λ_m is the mean free path in air.

The particle deposition fraction (DF) is defined as

$$DF = \frac{\text{Number of deposited particles in a specific region}}{\text{Number of particles entering the trachea}} \times 100\%. \tag{6}$$

2.3. Matching Reynolds and Stokes numbers

Transient inspiratory airflow fields are discussed in Part I. The particle deposition fractions for transient inhalation were found to be close to matching steady-state particle DFs when equivalent Reynolds and Stokes numbers were employed. The matching dimensionless groups can be evaluated as follows:

$$Re_{\text{match}} = C(Re_{\max} + Re_{\text{mean}}) \tag{7a}$$

and

$$St_{\text{match}} = C(St_{\max} + St_{\text{mean}}) \tag{7b}$$

where the maximum and mean parameter values correspond to the given inhalation waveform, the Stokes number is defined as $St = \rho_p d_p^2 U/(18\mu D)$ and ρ_p is the particle density, D is the tube diameter. Indeed, the results in Section 3.1 show that matching steady-state simulations with Re_{match} and St_{match} generate very similar segmentally averaged deposition fractions when compared to the actual transient inspiratory flow.

2.4. Numerical method

As mentioned in Part I, the commercial software Solidworks (Solidworks Corparation, Concord), Cadfix (ITI, Milford) and Gridpro (Program Development Company, White Plains) were employed to generate the smooth 3-D flow domain and finite volume mesh. The structured mesh was then read by the in-house code CFPD (Computational Fluid and Particle Dynamics) which outputs the flow field. The air velocities and associated domain geometry information are input to the particle trajectory solver F90, a module of CFPD for particle transport and deposition, developed by Buchanan [27] and Longest [28]. Specifically, the particle trajectory equation was solved by using an improved second-order Euler predictor-corrector method [29]. Assuming a randomized distribution, 106,600 microparticles, $d_p = 3$ μm to 10 μm were released at the trachea inlet. When an additional 50% of particles were released at the inlet, the resulting difference was less than 0.5%. The accuracy of the CFPD module F90 has been verified by Longest et al. [29] and Zhang et al. [30].

In the F90 code, the movement of each particle is separately calculated. At each time level, the current position of a particle is checked. If a particle's center locates within its radius from the stationary moist surface, i.e., airway wall, particle deposition is assumed. A sufficient number of iteration steps is set to guarantee realistic and accurate simulations. The trajectory calculation of a particle is terminated if the particle touches the wall, it flows out of the domain, or the maximum number of iteration steps has been reached. For this demanding simulation task, parallel computation was implemented with MPI (Message Passing Interface), i.e., appropriate data transfer between processors. While the computer simulation model was validated with experimental data in Part I for airflow, several microparticle deposition

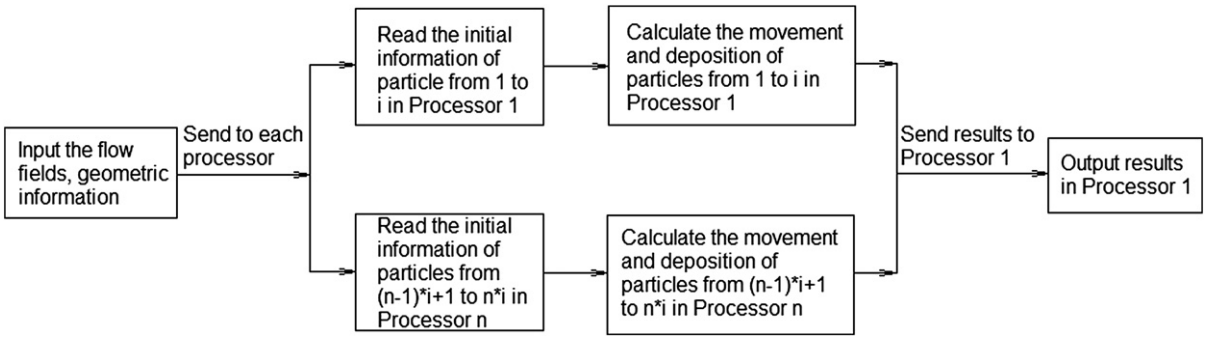

Fig. 2. Parallel simulation process flow chart.

comparisons have been documented by Zhang et al. [30]. The information of the airflow field and domain geometry is input to the particle program. Processor n solves the location (and deposition) of particles from $(n-1)i+1$ to ni after reading the corresponding initial particle information, where i is the order of a particle. All results are sent to Processor 1 which outputs the final data (see Fig. 2). Currently, particle bouncing and particle-to-particle collisions are not included because it is assumed that particles deposit when they touch the moist airway surface and inhaled particle stream is dilute.

3. Results and discussion

3.1. Transient and matching steady inhalation

As stated in Part I, the inlet velocity profiles were determined via analytical expressions for transient fully-developed flow in a straight tube [11]. Assuming parabolic particle inlet distributions, transient inhalation as well as matching steady air-particle flow was simulated. The particle deposition fractions for a typical Stokes number range of $0.025 \leqslant St_{\text{trachea}} \leqslant 0.102$ are shown in Figs. 3(a)–3(h) for smoothed trachea. As indicated in Part I, the airflow patterns are similar for different inlet Reynolds numbers. Thus, equivalent steady Reynolds numbers, as well as Stokes numbers, which generate the same particle deposition fractions (DFs) as they occur during transient inhalation, should exist. Concerning Eqs. (7a) and (7b), Zhang et al. [31] found the coefficient C to be 0.5 for Weibel's symmetric model. For the present more complex model, C is 0.535 where $Re_{\text{mean}} = 1201$ and $Re_{\text{max}} = 1544$. Indeed, the particle deposition fractions under matching steady-state condition are close to the ones for transient inhalation (see Figs. 3(a)–3(h)). For the most part, the difference is less than 5%. The two DF-error values greater than 10% appear in the bifurcation region F where only very few particles deposit. In general, the use of Eqs. (7a) and (7b) allow representation of corresponding smooth cyclic inhalation and hence major savings in computer resources.

3.2. Influence of inlet conditions on particle deposition

Assuming a parabolic inlet velocity profile, Figs. 4(a) and 4(b) show 3-D front and back views of particle deposition patterns, while Figs. 5(a) and 5(b) illustrate the results using the realistic inlet velocity profile, both for the out-of-plane configuration with $Re_{\text{in}} = 1201$. The particle DFs, although always lower for the realistic inlet velocity profile, are somewhat close for the two cases when considering a typical range of Stokes numbers (see Table 1). The main particle deposition characteristics are the same, i.e., most particles deposit at the carinal ridges while fewer particles deposit on the outer walls due to secondary flows. However, the particle deposition patterns at a specific position can be different. For example, at the first divider region, it can be observed that local wall concentrations are influenced by the form of inlet condition (compare amplified pictures in Figs. 4(a) and 5(a)). Specifically, fewer particles deposit at the carinal ridge for the realistic inlet flow because: (i) the axial velocity, responsible for particle impaction onto the carinal ridge, is lower; and (ii) upstream the secondary flow is stronger, which causes more particles to move away from the center before they collide with the carinal ridges. The local particle deposition differences lead to measurable discrepancies in total deposition fractions as summarized in Table 1. Clearly, assuming an idealized parabolic inlet profile, particle DFs are overpredicted, where for larger Stokes numbers the ΔDF-values increase; but, the relative differences are about 10% for all cases.

Table 1
Total deposition fraction for two different inlet velocity profiles (out-of-plane model)

St_{trachea}	Particle deposition fraction (%)	
	Parabolic	Realistic
0.025	17.7	16.1
0.051	27.8	24.7
0.076	40.3	36.2
0.102	56.1	49.0

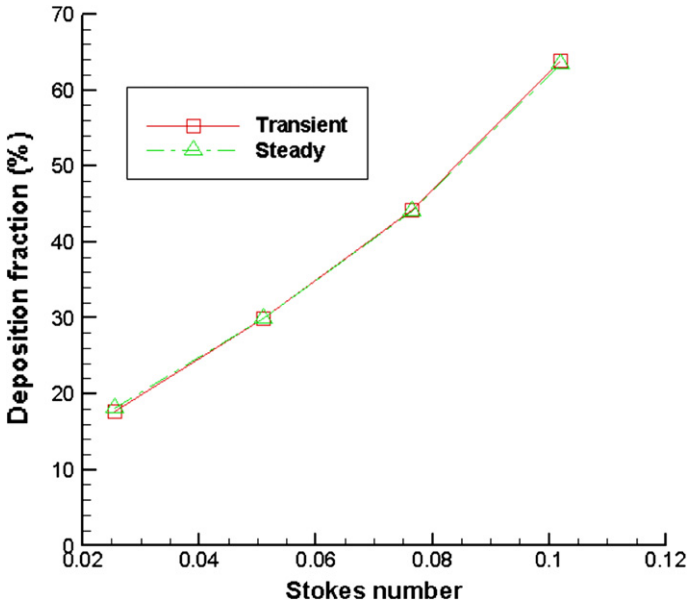

(a) Total deposition fraction

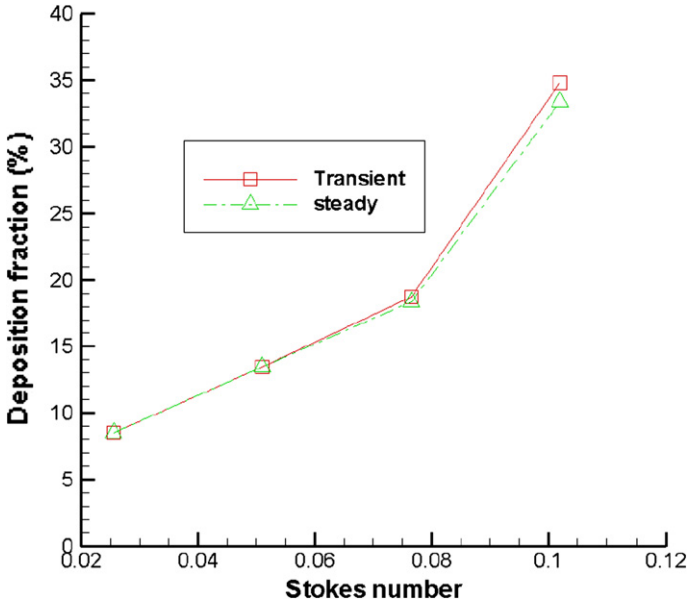

(b) Region A

Fig. 3. Particles deposition fractions in each bifurcation region (see Fig. 1(b)) (out-of-plane, cyclic case, $Re_{\text{in,mean}} = 1201$).

3.3. Geometric influences on particle deposition

In this section, geometric influences on particle deposition patterns are discussed. The effect of the spatial angle is first investigated by comparing results for the in-plane and out-of-plane configurations; then, the influence of tracheal rings is analyzed.

3.3.1. In-plane model vs. out-of-plane model

Most researchers considered particle deposition for in-plane configurations. Thus, assuming the realistic velocity inlet profile, the geometric effects, i.e., spatial angles, on deposition fractions are compared. Generally, most micropar-

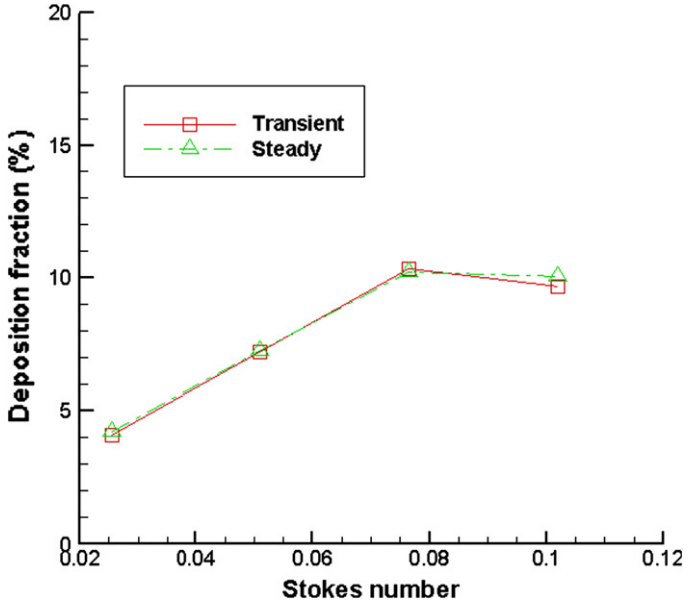

(c) Region B

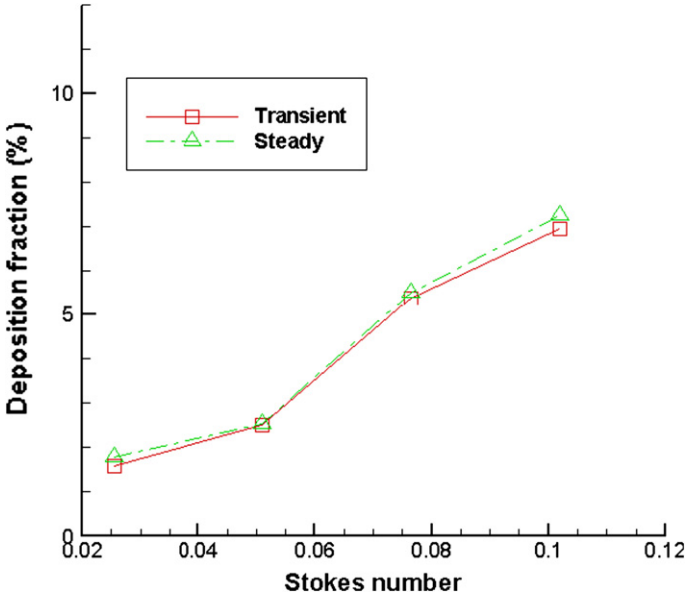

(d) Region E

Fig. 3 (*continued*).

ticles deposit on carinal ridges due to inertial impaction, while some particles may land on the surface of inside/outside curved tubes because of secondary flows in both models (see Figs. 1(a) and 1(d)). However, as expected, the particle depositions are quite asymmetric around both the carinal ridges and branches in the realistic airways.

Generally, in the out-of-plane airway particles deposit to a less extent at the carinal ridges, which is mainly due to the impaction of airflow. In contrast, more particles deposit along the tubular walls, induced by stronger local secondary flows (see Part I). The different axial and secondary flows in the out-of-plane model result in a higher total deposition fraction when compared to the in-plane configuration. However, as the Stokes number increases, the effect of axial flows increases and hence the differences between the two morphologies become smaller. In summary, the

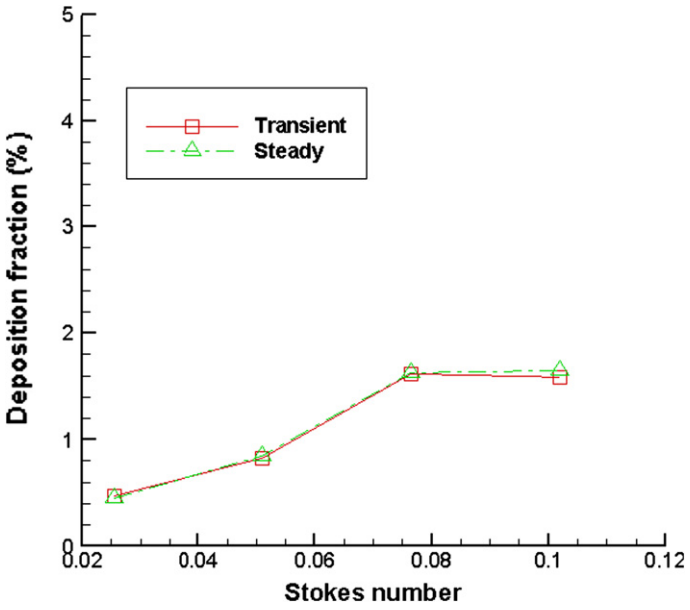

(e) Region C

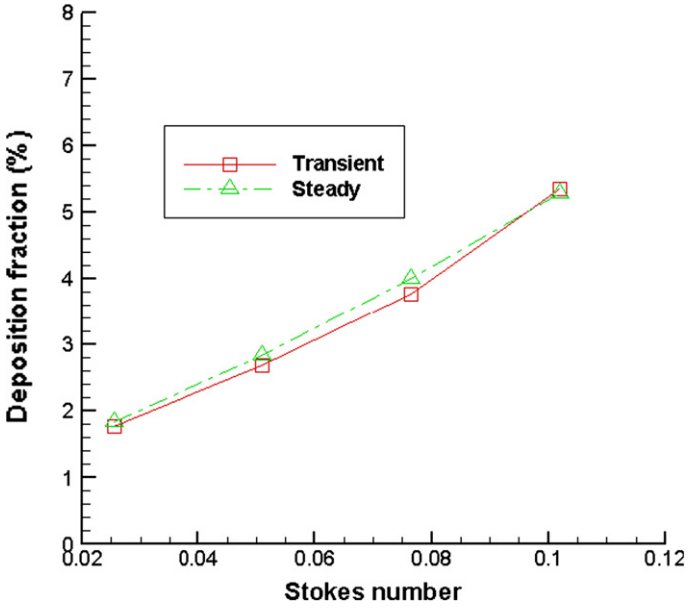

(f) Region D

Fig. 3 (*continued*).

total particle deposition fraction is higher in the out-of-plane than in the in-plane model for all cases studied (see Fig. 6(a)). This is consistent with results given for symmetric airway configurations (see [32]).

The situation becomes more complex when focusing on local DFs at each bifurcation region (see Figs. 6(b) to 6(h)). In Regions A, B and G, the DFs for the out-of-plane case are higher than those for the in-plane case, mainly due to locally stronger secondary flows. In Regions D, E and F, the DFs are larger in the out-of-plane model for small Stokes numbers; however, the DF-values are lower as the Stokes number increases. This is probably because the secondary flows in the in-plane model are weaker, shifting only the smaller particles from the center towards the side, before they impact with carinal ridges. The larger particles are less affected by weaker secondary flows. The variations in local DFs in Region C are more complex because both the bifurcation angle and the spatial angle are large. The DF

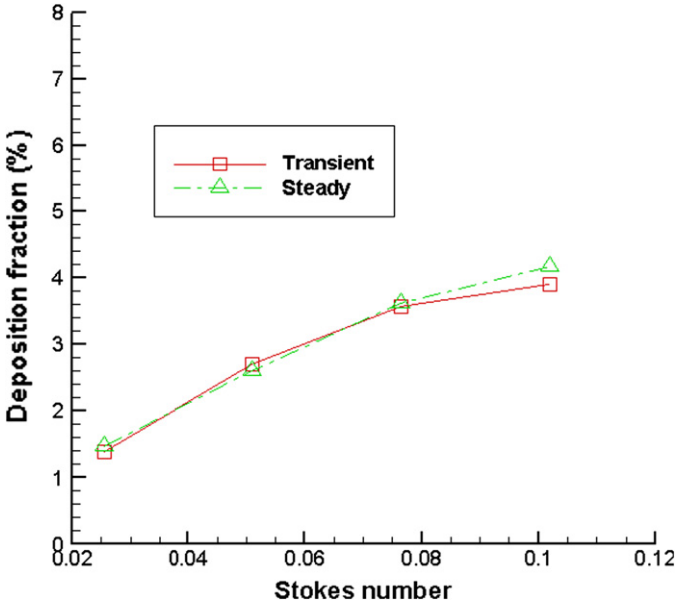

(g) Region G

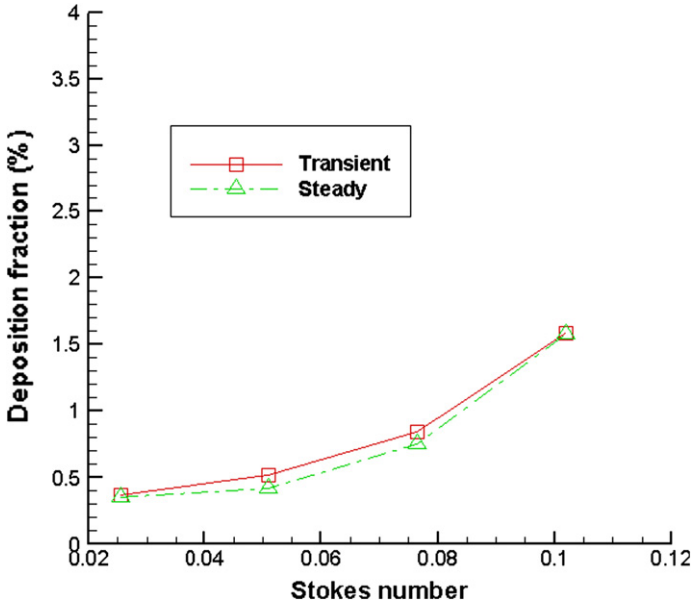

(h) Region F

Fig. 3 (*continued*).

is initially larger in the out-of-plane model and then becomes smaller. After a certain St-value, the DF is again higher. A possible reason for the last variation is that fewer particles enter Region C of the in-plane model.

3.3.2. The influence of cartilaginous rings in the out-of-plane model

Figs. 6(a)–6(h) also show the effect of tracheal rings on particle deposition fractions for the out-of-plane model with the realistic inlet condition ($Re_{in} = 1201$). For example, in the bifurcation region A close to the trachea, the influence of the cartilaginous ring structure is significant: the DF is obviously higher than when a smooth windpipe is assumed. In bifurcation region E, the DFs are quite similar between the surface configurations, i.e., with and without rings, because the secondary flow patterns as well as the axial velocities approaching the carinal ridges are quite similar.

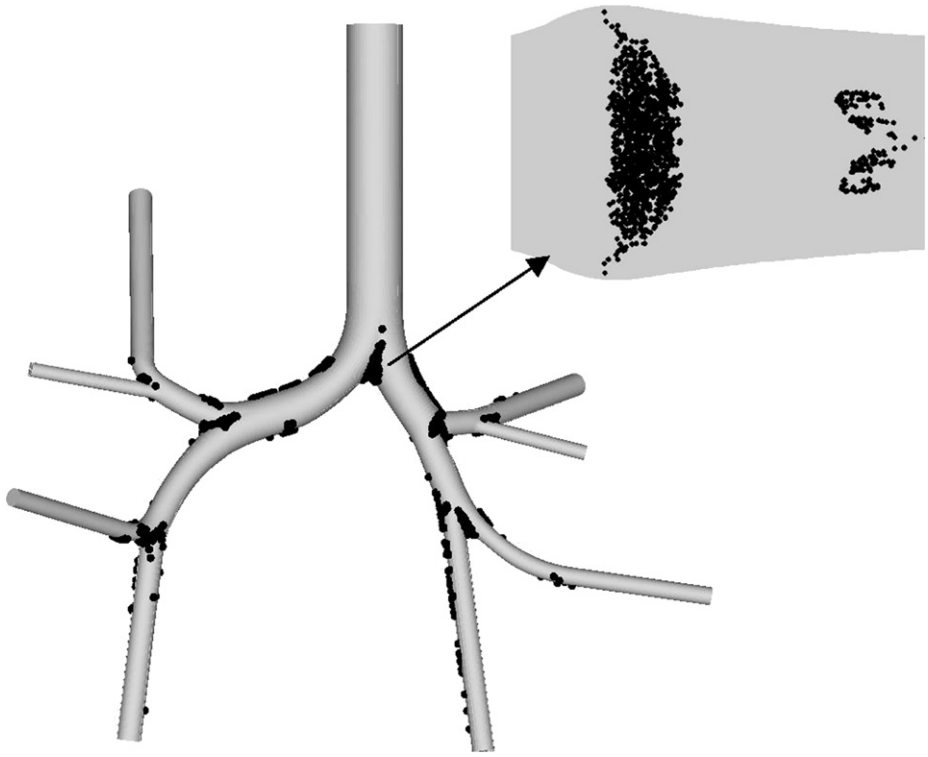

(a) front-view

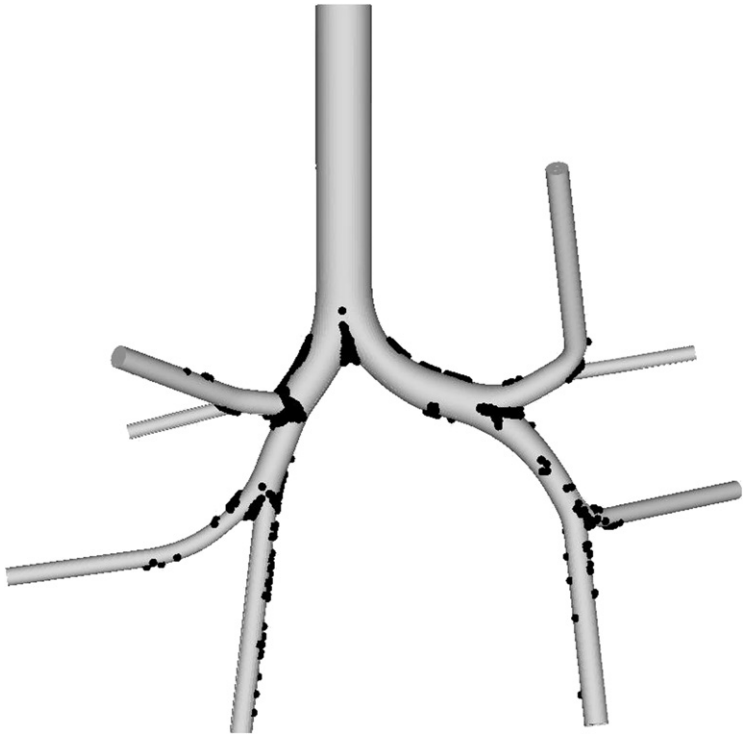

(b) back-view

Fig. 4. 3D visualizations of particle deposition for G0–G3 model (out-of-plane, steady-state case, parabolic inlet condition, $Re_{\text{in}} = 1201$, $St_{\text{trachea}} = 0.051$).

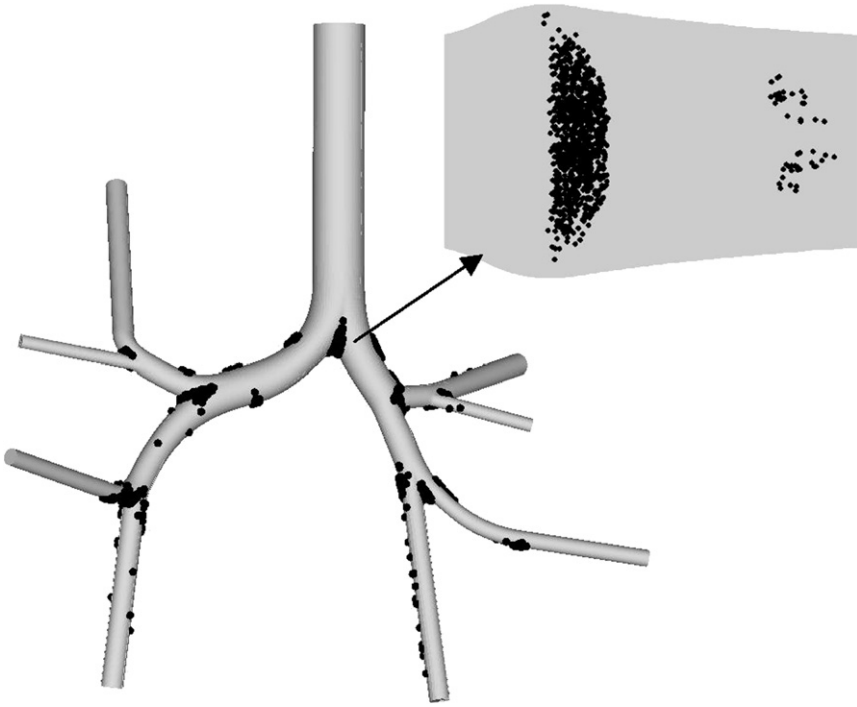

(a) front-view

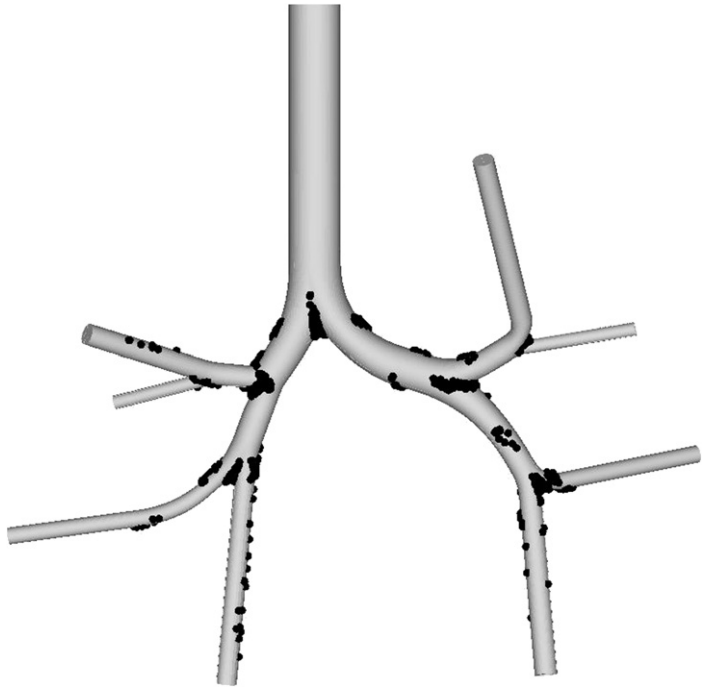

(b) back-view

Fig. 5. 3D visualizations of particle deposition for G0–G3 model (out-of-plane, steady-state case, realistic inlet condition, $Re_{\text{in}} = 1201$, $St_{\text{trachea}} = 0.051$).

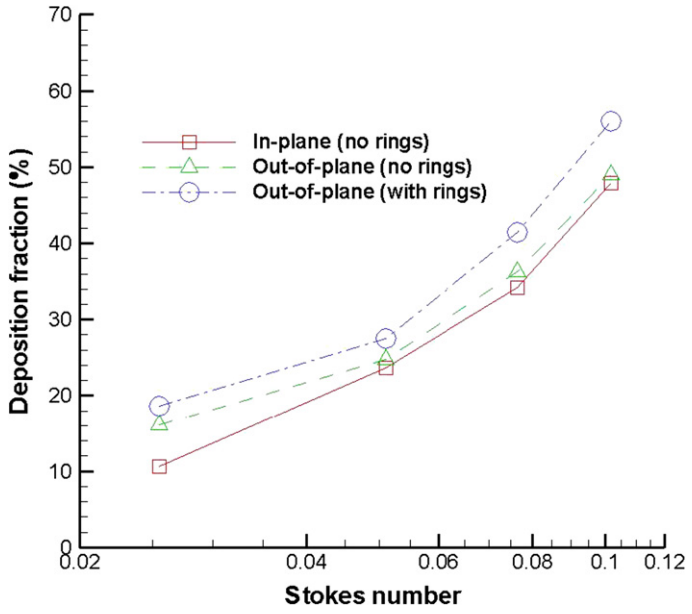

(a) Total deposition fraction

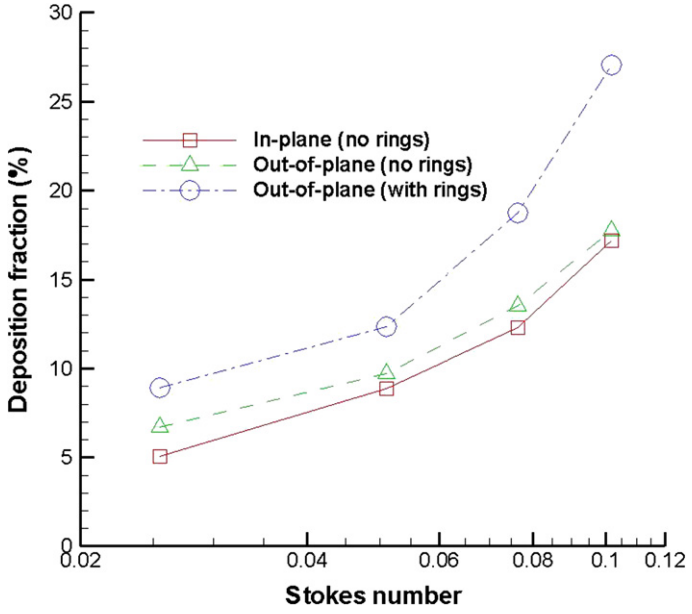

(b) Region A

Fig. 6. Particles deposition fractions in each region (see Fig. 1(b)) in different models (steady-state case, realistic inlet condition, $Re_{in} = 1201$).

Such phenomena are also observed for Region B. For Regions C, D, F and G, the DFs can be lower (F, G), higher (D), or similar (C) in the model with tracheal rings, although the flow patterns are similar.

3.4. Comparisons with other models

Subject variability and resulting differences in local vs. segmentally averaged particle deposition values are of great interest. Focusing on Region A (see Fig. 1(b)) for which experimental and theoretical DF data are available, Fig. 7 provides a comparison with results of Zhou and Cheng [19], Zhang et al. [30], and Cai and Yu [33]. Specifically,

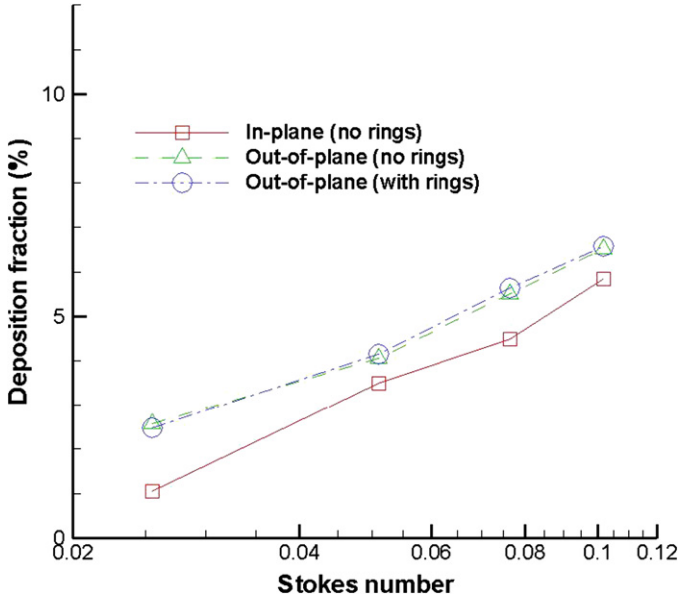

(c) Region B

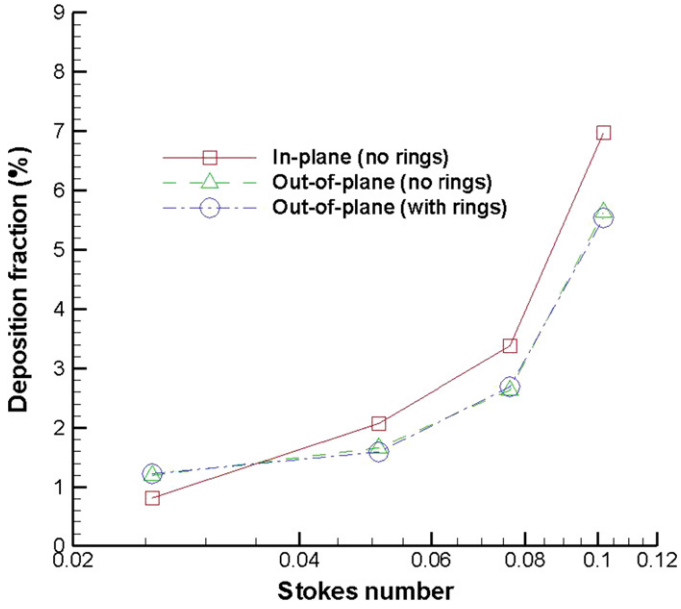

(d) Region E

Fig. 6 (*continued*).

Cai and Yu [33] developed a correlation (Eq. (8)) to predict particle deposition in an idealized symmetric airway bifurcation based on a "stopping-distance" concept.

$$DF = \frac{4\sin\alpha}{\pi(R/R_0)}St \tag{8}$$

where α is the bifurcation angle, R and R_0 are the radii of daughter and parent branches, respectively, and St is the Stokes number at the inlet of the parent branch. More recently, Zhou and Cheng [19] measured particle depositions in a realistic cast of a human upper lung airway. Zhang et al. [30] investigated computationally the DFs, using a modified oral airway cast with a Weibel Type A model attached. In the following comparison only deposition data equivalent to Region A were extracted for the last two sources.

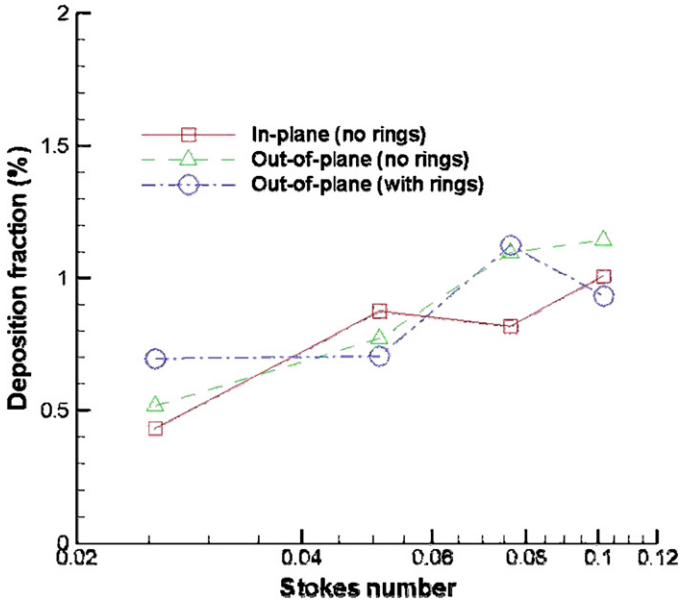

(e) Region C

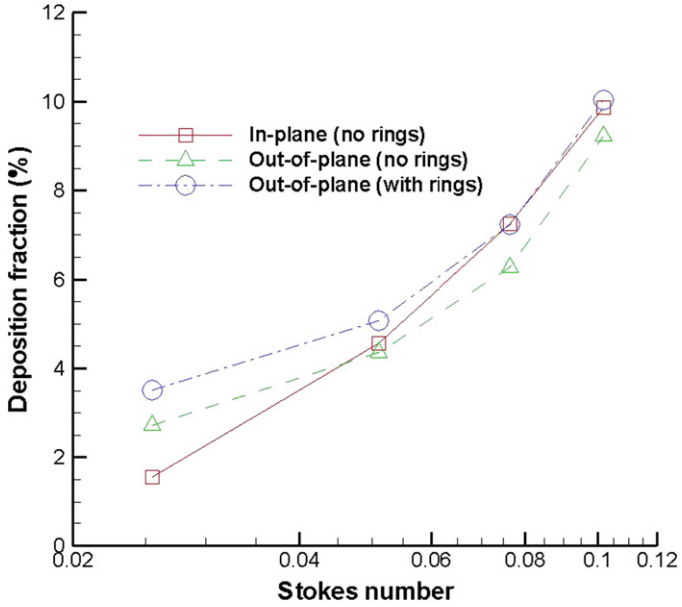

(f) Region D

Fig. 6 (*continued*).

The present results for Region A using the steady realistic velocity profile for the out-of-plane model without trachea rings, are in good agreement with the experimental data of Zhou and Cheng [19] and Eq. (7) of Cai and Yu [33]. Fig. 7 also displays data sets of particle deposition fractions in the first bifurcation region for the Weibel Type A model, which was investigated by Zhang et al. [30] for all flow rates (i.e., $Q_{\text{in}} = 15, 30, 60$ l/min). With the realistic upstream configuration used [30], the Weibel Type A model provides reasonable results for relatively low and high Stokes numbers. Differences are due to geometric characteristics and hence airflow effects on particle transport/deposition. For example, the two branching angles in the first bifurcation are 63 degrees and 35 degrees in the current realistic model while they are a uniform 30 degrees in the planar Weibel Type A model; thus, the influence

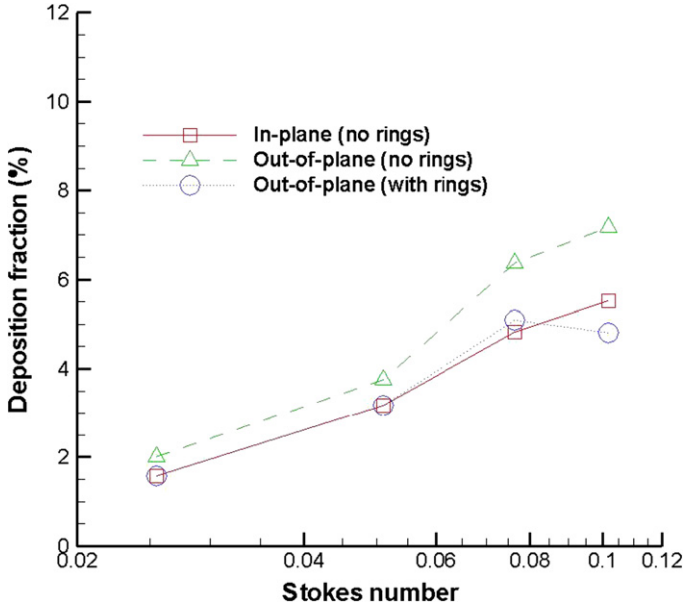

(g) Region G

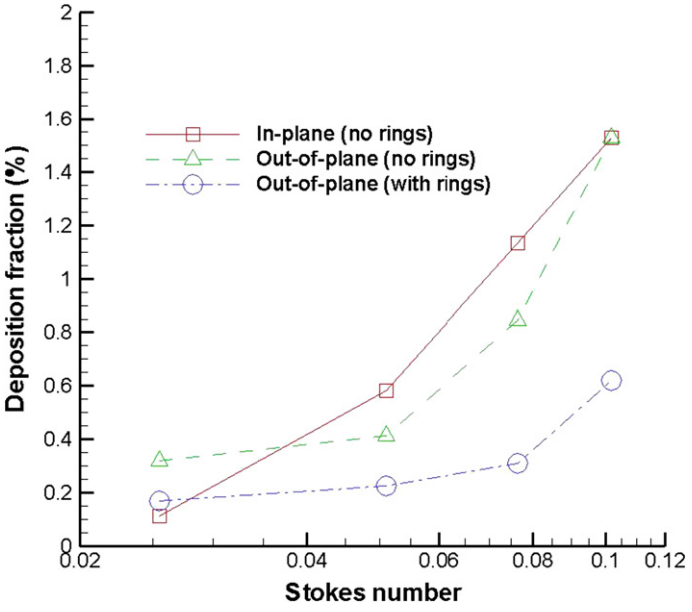

(h) Region F

Fig. 6 (*continued*).

of the branching angle is particularly important. In addition, in the current asymmetric model the radii of the daughter tubes are different, which leads to changes in airflow fields and hence particle distributions.

3.5. Microparticle deposition correlations for left and right lung

Employing the out-of-plane model without tracheal rings, the steady flow simulations have been performed for different inlet Reynolds number assuming the parabolic inlet profile. Figs. 8(a) and 8(b) show the particle deposition fractions in the left part (Regions B–D) and in the right part (Regions E–G) respectively. It is observed that the DFs in the left side are higher than in the right side as the geometry in the left side changes more dramatically, especially at

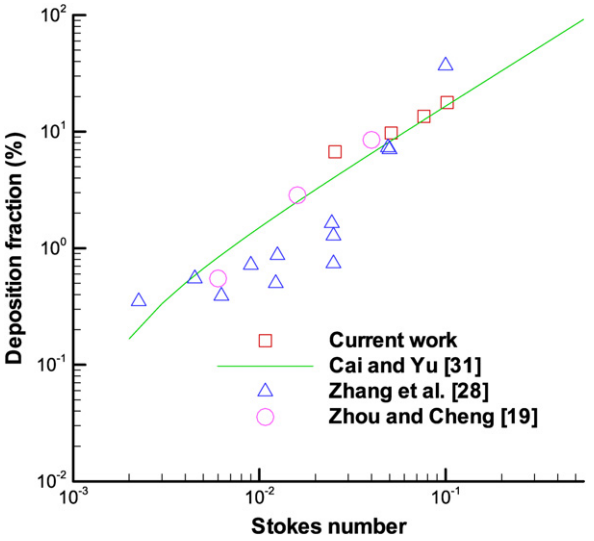

Fig. 7. Comparison of experimental and computational deposition results for bifurcation region A (steady-state case, realistic inlet condition, $Re_{\text{in}} = 1201$).

Table 2
Coefficients for Eq. (8)

Lung region	Coefficients									r^2
	a	b	c	d	e	f	g	h	i	
left	43.94	−1341.	73.037	2.013	0.2727	−6.530	6387.	0.0	0.0	0.981
right	7.283	−200.	8.2975	7.280	0.2078	−17.95	−1594.	24472.0	116.4	0.985

the second-order branches (compare Regions B and E), which causes both stronger axial and secondary flows in the left side.

Following Zhang et al. [31], a curve-fitted equation was developed to summarize the DF simulation results. Specifically,

$$DF = f_1(St_{\text{trachea}})\, f_2(Re_{\text{trachea}}) \tag{9a}$$

where

$$f_1(St) = \frac{a(St + f\,St^2 + i\,St^3)}{(h\,St^4 + g\,St^3 + b\,St^2 + c\,St + 1.0)} \tag{9b}$$

and

$$f_2(Re) = d(Re)^e. \tag{9c}$$

The lines shown in Figs. 8(a) and 8(b) represent the curve-fitted results. The coefficients a–i and the multiple determination coefficient (r^2) are given in Table 2. The good agreements indicate that the correlation functions can be used to evaluate microparticle depositions in different lung segments as a function of typical inlet Stokes and Reynolds numbers. The exhalation is not considered in the simulation.

4. Conclusions

In Part II, microparticle deposition for a typical Stokes number range, i.e., $0.025 \leqslant St_{\text{trachea}} \leqslant 0.102$, is discussed, based on airflow fields provided in Part I. The human lung airway model data were given by Horsfield et al. [14], Raabe et al. [25], and Zhang and Finlay [20].

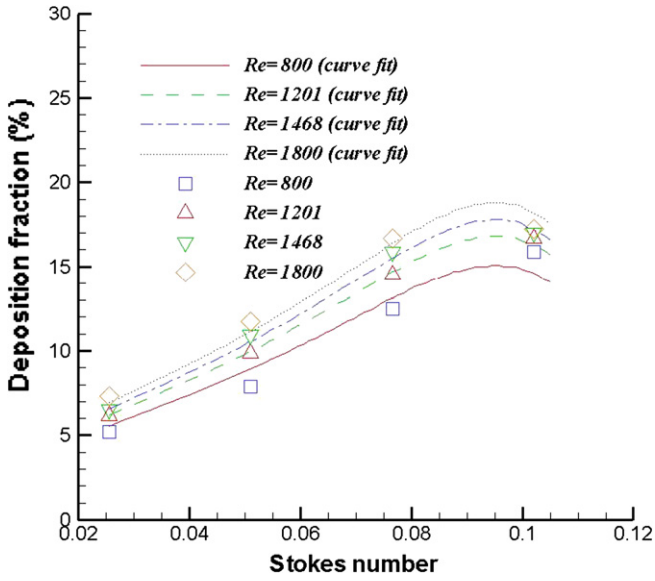

(a) left part

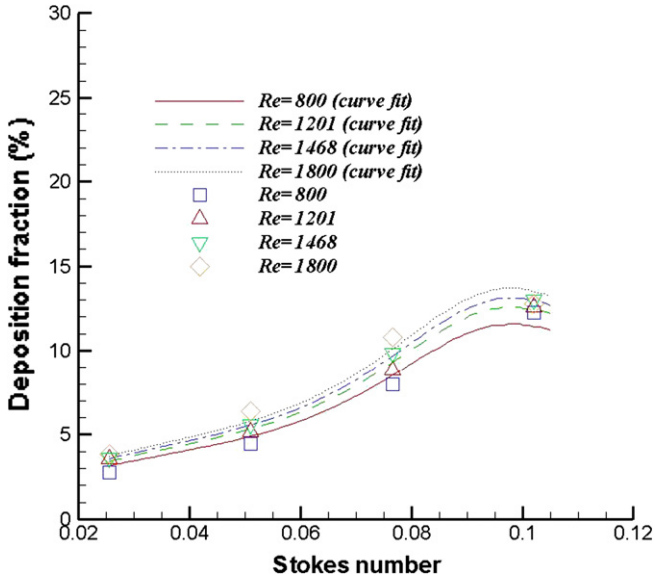

(b) right part

Fig. 8. Correlation for particle deposition fractions under different inlet Reynolds numbers.

The effects of transients, inlet conditions and geometric characteristics, i.e., spatial angle and tracheal ring structure have not been published before. For the representative, i.e., asymmetric and out-of-plane, model the following conclusion can be drawn. The human upper airway simulation results show that equivalent steady-state Reynolds and Stokes numbers can be found to match transient inhalation in terms of particle deposition fractions under moderate breathing condition ($Q_{\text{in}} = 15$ l/min). The specific velocity inlet profile influences particle deposition to a certain extent, e.g., the total particle DFs are higher when parabolic inlet profiles are assumed than realistic inlet velocity profiles. This indicates the kinematic upstream effects are important for particle deposition, although it has less an influence on the flow field. The spatial angle and tracheal ring structures further change local particle deposition concentrations when compared with simple geometric models. For all practical purposes, algebraic microparticle-deposition correlations, $DF = DF(St_{\text{trachea}}, Re_{\text{trachea}})$, have been obtained for both the left and right upper lung airways.

Presently, realistic inlet conditions have not been implemented for transient inhalation. However, in future work, realistic oral airways will be connected to the present trachea-G3 model under fully transient as well as equivalent steady-state conditions.

Acknowledgement

This work was sponsored by the Air Force Office of Scientific Research, Air Force Material Command, USAF, under grant number FA9550-04-1-0422 (Dr. Walt Kozumbo, Program Manager).

References

[1] International Commission on Radiological Protection (ICRP), Human Respiratory Tract Model for Radiological Protection, Publication 66, Ann. ICRP, Pergamon Press, Oxford, 1994, p. 456.
[2] C.A. Pope, D.W. Dockery, J. Schwartz, Review of epidemiological evidence of health effects of particulate air pollution, Inhal. Toxicol. 7 (1995) 1.
[3] S.J. Smith, J.A. Bernstein, Therapeutic uses of lung aerosols, in: A.J. Hickey (Ed.), Inhalation Aerosol: Physical and Biological Basis for Therapy, M. Dekker, New York, 1996, p. 233.
[4] I. Gonda, Particle deposition in the human respiratory tract, in: R.G. Crystal, J.B. West, E.R. Weibel, P.J. Barnes (Eds.), The Lung: Scientific Foundations, Lippincott-Raven Publishers, Philadelphia, 1997, p. 2289.
[5] A.A. Kinsara, R.V. Tompson, S.K. Loyalka, Computational flow and aerosol concentration profiles in lung bifurcations, Health Phys. 64 (1993) 13.
[6] B. Gatlin, C. Cuicchi, J. Hammersley, D. Olson, R. Reddy, G. Burnside, Particle path and wall deposition patterns in laminar flow through a bifurcation, in: ASME FED SM97, Vancounver, British Columbia, Canada, 1997, p. 1.
[7] T. Heistracher, W. Hofmann, Flow and deposition patterns in successive airway bifurcations, Ann. Occup. Hyg. 41 (1997) 537.
[8] L. Zhang, B. Asgharian, S. Anjilvel, Inertial deposition of particles in the human upper airway bifurcation, Aerosol Sci. Technol. 26 (1997) 97.
[9] J.K. Comer, C. Kleinstreuer, C.S. Kim, Flow structures and particle deposition patterns in double-bifurcation airway models. Part 2. Aerosol transport and deposition, J. Fluid Mech. 435 (2001) 55.
[10] M.J. Oldham, R.F. Phalen, T. Heistracher, Computational fluid dynamics predictions and experimental results for particle deposition in an airway model, Aerosol Sci. 32 (2000) 61.
[11] Z. Zhang, C. Kleinstreuer, C.S. Kim, Aerosol deposition efficiencies and upstream release positions for different inhalation modes in an upper bronchial airway model, Aerosol Sci. Technol. 36 (2002) 135.
[12] E.R. Weibel, Morphometry of the Human Lung, Academic, New York, 1963.
[13] C.V. Ertbruggen, C. Hirsch, M. Paiva, Anatomically based three-dimensional model of airways to simulate flow and particle transport using computational fluid dynamics, J. Appl. Physiol. 98 (2005) 970.
[14] K. Horsfield, G. Dart, D.E. Olson, Models of the human bronchial tree, J. Appl. Physiol. 21 (2) (1971) 207.
[15] J.R. Johnston, K.D. Isles, D.C.F. Muri, Inertial deposition of particles in human branching airways, in: W.H. Walton (Ed.), Inhaled Particles IV, Pergamon, 1977.
[16] C.S. Kim, A.J. Iglesias, Deposition of inhaled particles in bifurcating airways models: I. inspiratory deposition, J. Aerosol. Medicine 2 (1989) 1.
[17] C.S. Kim, D.M. Fisher, D.J. Lutz, T.R. Gerrity, Particle deposition in bifurcating airway models with varying airway geometry, Aerosol. Sci. Technol. 25 (1994) 567.
[18] C.S. Kim, D.M. Fisher, Deposition characteristics of aerosol particles in successively bifurcating airway models, Aerosol. Sci. Technol. 31 (1999) 198.
[19] Y. Zhou, Y.-S. Cheng, Particle deposition in a cast of human tracheobronchial airways, Aerosol Sci. Technol. 39 (2005) 492.
[20] Y. Zhang, W.H. Finlay, Measurement of the effect of cartilaginous rings on particle deposition in a proximal lung bifurcation model, Aerosol Sci. Technol. 39 (2005) 394–399.
[21] C.S. Kim, S.C. Hu, P. Dewitt, T.R. Gerrity, Assessment of regional deposition of inhaled particles in human lungs by serial bolus delivery method, J. Appl. Physiol. 81 (1996) 2203.
[22] Z. Zhang, C. Kleinstreuer, Transient airflow structures and particle transport in a sequentially branching lung airway model, Phys. Fluids 14 (2) (2002) 862.
[23] P.W. Scherer, F.R. Haselton, Convective exchange in oscillatory flow through bronchial-tree models, J. Appl. Physiol. 53 (1982) 1023.
[24] S. Mochizuki, Convective mass transport during ventilation in a model of branched airways of human lungs, in: Proceedings of PSFVIP-4, Chamonix, France, 2003.
[25] O.G. Raabe, H.C. Yeh, G.M. Schum, R.F. Phalen, Tracheobronchial geometry, i.e. human, dog, rat, hamster LF-53, Lovelace Foundation for medical Education and Research, Albuquerque, NM, 1976.
[26] R. Clift, J.R. Grace, M.E. Weber, Bubbles, Drops, and Particles, Academic Press, New York, 1978.
[27] J.R. Buchanan, Computational particle hemodynamics in the rabbit abdominal aorta, Ph.D. dissertation, MAE Dept., NC State University, Raleigh, NC, 2000.
[28] P.W. Longest, Computational analyses of transient particle hemodynamics with applications to femoral bypass graft designs, Ph.D. dissertation, MAE Dept., NC State University, Raleigh, NC, 2002.

[29] P.W. Longest, C. Kleinstreuer, J.R. Buchanan, Efficient computation of micro-particle dynamics including wall effects, Computers and Fluids 36 (2004) 577.
[30] Z. Zhang, C. Kleinstreuer, J.F. Donohue, C.S. Kim, Comparison of micro- and nano-size particle depositions in a human upper airway model, Aerosol Sci. 36 (2005) 211.
[31] Z. Zhang, C. Kleinstreuer, C.S. Kim, Aerosol deposition fractions and upstream release positions for different inhalation modes in an upper bronchial airway model, Aerosol Sci. Technol. 36 (2002) 828.
[32] J.K. Comer, C. Kleinstreuer, C.S. Kim, Flow structures and particle deposition patterns in double-bifurcation airway models. Part 2. Aerosol transport and deposition, J. Fluid Mech. 435 (2001) 55.
[33] F.S. Cai, P.C. Yu, Inertial and interceptional deposition of spherical particles and fibers in a bifurcating airway, J. Aerosol Sci. 19 (1988) 679.
[34] E.E. Michaelides, Review – the transient equation of motion for particles, bubbles and droplets, J. Fluids Engrg. 119 (1997) 233.